

Cite this article as: Chen Haibo, Zheng Jingwu, Fu Yongcheng, et al. Preparation and Characterization of Copper-Graphene Composite Films on Sintered NdFeB Surface[J]. Rare Metal Materials and Engineering, 2021, 50(12): 4306-4313.

ARTICLE

Preparation and Characterization of Copper-Graphene Composite Films on Sintered NdFeB Surface

Chen Haibo^{1,2}, Zheng Jingwu¹, Fu Yongcheng¹, Liu Youhao³, Yi Xiaofei³, Chen Jingwu³, Qiao Liang¹, Huang Xiulian³, Ying Yao¹, Cai Wei¹, Li Wangchang¹, Yu Jing¹

¹Research Center of Magnetic and Electronic Materials, College of Materials Science and Engineering, Zhejiang University of Technology, Hangzhou 310014, China; ²College of Mechanical Engineering, Zhejiang University of Technology, Hangzhou 310000, China; ³State Key Laboratory of Rare Earth Permanent Magnet Materials, Earth-Panda Advance Magnetic Material Co., Ltd, Hefei 231500, China

Abstract: Corrosion resistance of rare earth permanent magnet material NdFeB was achieved by electrodeposited Cu-graphene (Cu-GR) composite films. The impact of the films on corrosion performances was studied by examining the morphology, water contact angle, and surface microhardness. The results show that the hydrophobicity and the hardness are enhanced as the concentration of graphene in the plating solution increases from 0 g·L⁻¹ to 0.9 g·L⁻¹. The characterization through SEM/EDS and XPS verifies the uniform dispersion of graphene sheets in the electrodeposited coating and the composition of Cu-GR composites. The electrochemical performance of the Cu-GR composite coating was investigated by potentiodynamic polarization curves and electrochemical impedance spectroscopy (EIS), and it is demonstrated that the electrochemical performance becomes more stable and the corrosion resistance is improved with the addition of graphene in the composites. For the sintered NdFeB samples coated with Cu-GR composite films with different graphene concentrations the best protective effect is obtained for the film prepared from the plating solution with a graphene concentration of 0.3 g·L⁻¹.

Key words: Cu-graphene; composite coating; corrosion resistance; NdFeB

NdFeB magnets have been extensively used and attracted significant interest in both research and industry owing to their excellent properties^[1-4], including outstanding maximum magnetic energy product (BH_{\max}), relatively high coercivity (H_c), and lower content of precious rare-earth elements per molecular mass than other hard magnets such as SmCo₅^[1]. They are widely applied in various emerging and conventional industries, such as electric vehicles, wind power generators, energy-saved motors, medical apparatus, acoustics, and aerospace and military industry^[5]. However, the chemical stability of sintered NdFeB magnets is poor due to the presence of rare-earth element neodymium (Nd)^[6,7], which is one of the most electrochemically active metals^[8]. Furthermore, NdFeB is a multiphase structure that possesses large chemical potential differences between the phases^[9,10], leading to intergranular corrosion, especially for the Nd-rich

phase (Nd₄Fe)^[8]. These bottlenecks limit their practical applications, and thus, related research on coating has attracted widespread attention^[5,6]. Coating bulk magnet is one of the most promising methods to avoid the disadvantageous effects of corrosive environments, and electrodeposition is one of the most commonly used methods for preparing metal matrix composite coatings^[11]. Metal coatings, such as Cu, Cr, Al, Zn, Ni, are widely studied. Among them, the Cu coating possesses excellent compactness and can be electrodeposited by non-corrosive alkaline cyanide-free plating system^[12,13], but its corrosion resistance is insufficient. Thus, improving the corrosion resistance of Cu coating is of great importance.

Graphene (GR) is considered promising due to its unique physicochemical properties and ease of synthesis^[14-17]. Corrosion inhibition of metal materials using GR-based composite coatings^[18-28] is an emerging field. For example,

Received date: April 28, 2021

Foundation item: National Natural Science Foundation of China (51871201); Key R&D Project of Zhejiang Provincial Department of Science and Technology (2021C01172)

Corresponding author: Zheng Jingwu, Ph. D., Research Center of Magnetic and Electronic Materials, College of Materials Science and Engineering, Zhejiang University of Technology, Hangzhou 310014, P. R. China, Tel: 0086-571-88320142, E-mail: zhengjw@zjut.edu.cn

Copyright © 2021, Northwest Institute for Nonferrous Metal Research. Published by Science Press. All rights reserved.

metal-GR composite coatings (for instance, Cr-GR^[27], and Sn-GR^[28]) have been applied for steel^[29,30], Ni^[31] and other metals to protect the underlying metals from corrosive attacks. Incorporating GR sheets into the metal film and forming metal-GR composite layer is an effective approach to protect the substrate from corrosion.

In this work, we dispersed graphene sheets into electrodeposited Cu coating to form a Cu-GR composite film which was coated onto the sintered NdFeB surface to enhance the corrosion resistance of the magnets. The influence of the concentration of graphene added in the plating solution was investigated, and the mechanism of improving the corrosion resistance of the resulting Cu-GR coatings was also studied.

1 Experiment

The composite material was prepared by electrodeposition with stirring and ultrasonication. The electroplating solution was composed of 1-hydroxyethylidene-1,1-diphosphonic acid (HEDP, 100 g·L⁻¹), CuSO₄·5H₂O (40 g·L⁻¹), KOH (80 g·L⁻¹), K₂CO₃ (100 g·L⁻¹), triethanolamine (TEA, 20 mL·L⁻¹), and sodium dodecyl sulfate (0.5 g·L⁻¹). Besides, the graphene sheets (0, 0.3, 0.6, and 0.9 g·L⁻¹) were added and dispersed into the solution. In the process of preparing the Cu-GR composite material by electrodeposition, the current density was 2 A·dm⁻², and the electrodeposition time was 10 min. Furthermore, the experimental temperature was controlled at 20±1 °C, and the ultrasonic power was 480 W.

Morphological characteristics and the elemental distribution of Cu and C were characterized using scanning electron microscopy/energy-dispersive X-ray spectrometry (SEM/EDS; FEI, Nova NanoSEM 450). A laser particle size analyzer (S3500 Bluewave) was used to measure the particle size distribution of the graphene sheets under ultrasound. An optical contact angle tester (OCA30) was used to test the water contact angle of the sample surface. The hardness values of the composites were tested by the microhardness tester (HVT-1000) at a loading force of 2.94 N for a dwell time of 10 s. Furthermore, the Cu-GR composites were investigated using X-ray photoelectron spectra (XPS, Kratos Axis Ultra DLD). The potentiodynamic polarization curves and electrochemical impedance spectroscopy (EIS) were applied to evaluate the electrochemical performance and the corrosion resistance on an electrochemical workstation (Ivium V38108). Three-electrode system was used for the electrochemical measurement and the electrolyte was 3% sodium chloride solution. The coated NdFeB magnet, the platinum electrode, and the saturated calomel electrode (SCE) were used as the working electrode, the auxiliary electrode, and the reference electrode, respectively. The potentials mentioned in the text were relative to the reference electrode potential. The corresponding anodic polarization scan rate was 5 mV·s⁻¹, and the AC impedance amplitude was 10 mV. The impedance test frequency range was 10 to 0.01 kHz. All electrochemical tests were conducted at 25±2 °C.

2 Results and Discussion

2.1 Morphology and particle size distribution of GR sheets

The microscopic morphology and the particle size distribution of the graphene raw material were characterized, as shown in Fig. 1. The SEM image (Fig. 1a) shows that the graphene sheets are translucent, parts of which consist of creases and folds. The graphene sheets are agglomerated into particles with a diameter of about 5 μm. To further characterize the size of the graphene sheets, the particle size distribution was determined by the laser particle sizer, as shown in Fig. 1b. The values of the 10th percentile size (D_{10}), 50th percentile or average particle size (D_{50}), and 90th percentile size (D_{90}) are D_{10} =2.3 μm, D_{50} =3.9 μm, and D_{90} =7.6 μm, respectively. This indicates that most of the graphene sheets are in the size range of 2~8 μm, consistent with the SEM results.

2.2 Microscopic structures and properties of Cu-GR composite surface

The Cu-GR composite was prepared on the surface of the sintered NdFeB matrix, and the microscopic structures and properties were analyzed. Fig. 2 shows the SEM images of the composite prepared on a smooth NdFeB substrate with different graphene concentrations. The images were observed under magnifications of 5000× and 20000×. Fig. 2a~2d (5000×) show that the composite particles are remarkably refined and the surface exhibits a fine pore-like morphology as the graphene concentration in the bath increases. In Fig. 2e~2h (20000×), rough and undulating appearance is observed on the surface of the composite material, indicating the formation of a superhydrophobic microscopic undulating structure. The surface relief structure becomes more obvious as the

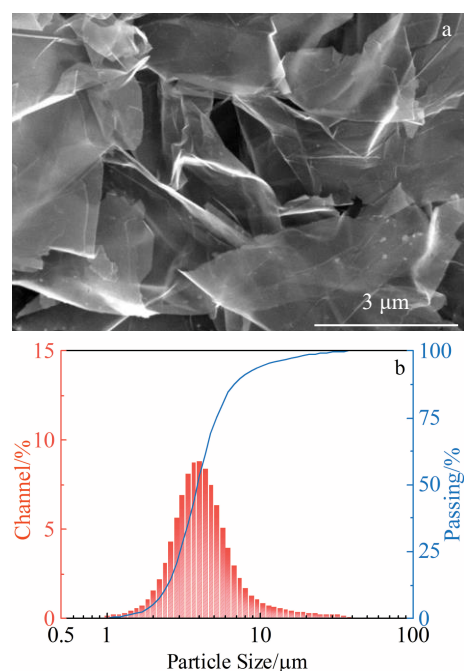


Fig.1 SEM morphology (a) and particle size distribution (b) of GR sheets

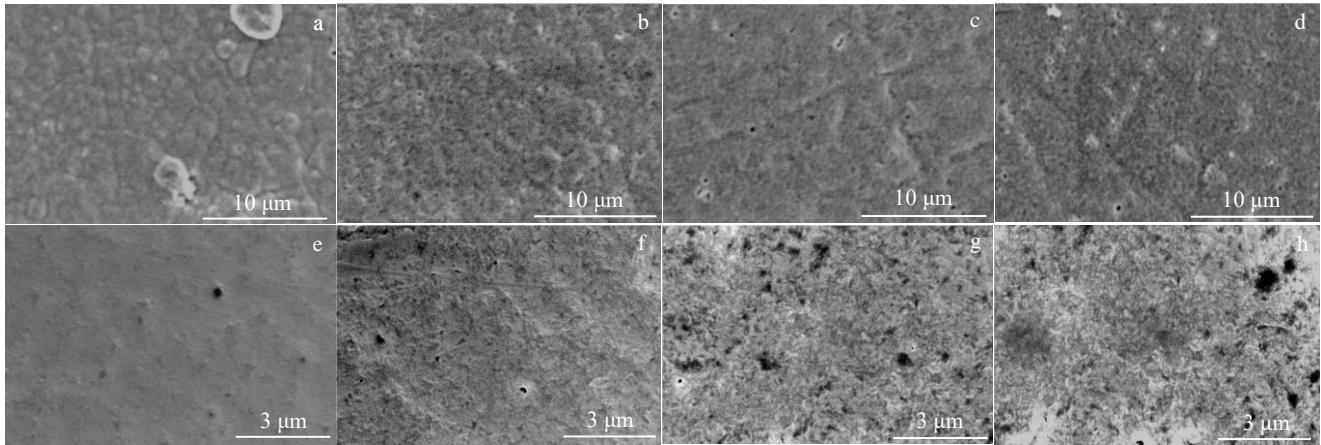


Fig.2 SEM images of surface topography of Cu-GR composites with different graphene concentrations: (a, e) $0 \text{ g}\cdot\text{L}^{-1}$, (b, f) $0.3 \text{ g}\cdot\text{L}^{-1}$, (c, g) $0.6 \text{ g}\cdot\text{L}^{-1}$, and (d, h) $0.9 \text{ g}\cdot\text{L}^{-1}$

concentration of graphene in the plating solution increases. Furthermore, graphene itself possesses highly hydrophobic properties^[32], which plays an important role in corrosion resistance, especially in humid environments^[33,34]. For these reasons, the water contact angle on the surface of the samples was examined, as shown in Fig. 3. As the graphene concentration in the composite material increases, the values of the surface water contact angle of the prepared composite material tend to increase, indicating enhanced hydrophobicity. Furthermore, the surface hardness was tested. As shown in Fig.4, the hardness increases from 1780 to 2870 MPa as the graphene concentration increases from $0 \text{ g}\cdot\text{L}^{-1}$ to $0.9 \text{ g}\cdot\text{L}^{-1}$. To investigate the toughness and compactness of the Cu-GR composite materials, the torn cross-sectional SEM images are shown in Fig.5. Fig.5a shows that the torn cross-section of the sample without graphene has a rugged appearance, which is attributed to the excellent toughness and ductility of pure Cu. In contrast, for the composite samples containing graphene, especially when the graphene concentration reaches $0.9 \text{ g}\cdot\text{L}^{-1}$, the torn cross-sections are much smoother, and there is a tendency to brittle fracture. This indicates that the hardness of the Cu-GR composite increases, and the toughness is reduced with the increase of graphene concentration. Besides, no internal pores are observed inside the Cu-GR composite (Fig.5b~5d), indicating that the fabricated composites possess excellent compactness. In summary, the Cu-GR composites form compact protective films, and the hardness and the hydrophobicity are enhanced as the concentration of graphene increases.

2.3 Distribution of graphene sheets in Cu-GR composite coating

To investigate the distribution of graphene in the composite material, the elemental distributions and atomic percentages of C and Cu in different samples were characterized using SEM/EDS. As shown in Fig.6a, Cu is found to be the major element in the electrodeposited coating in the absence of graphene. A very small amount of C is detected which might be derived from the dispersant of sodium dodecyl sulfonate in

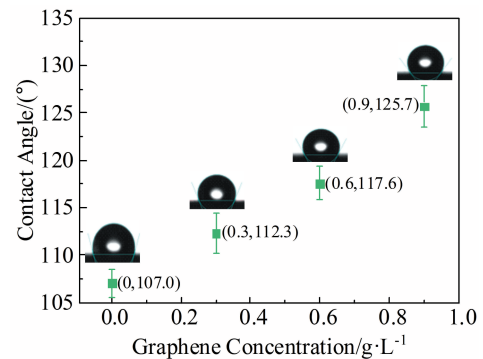


Fig.3 Surface water contact angle of Cu-GR composites with different graphene concentrations

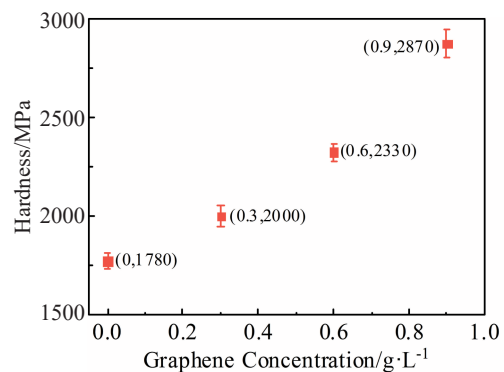


Fig.4 Surface microhardness of Cu-GR composites with different graphene concentrations

the plating solution. Fig.6 shows that the proportion of C in the composite increases as the amount of graphene in the plating solution increases, and the proportion of Cu decreases accordingly. The distributions of C and Cu in the composite material are relatively uniform, indicating that the graphene sheets are uniformly dispersed in the composite material, as shown in Fig.6b~6d.

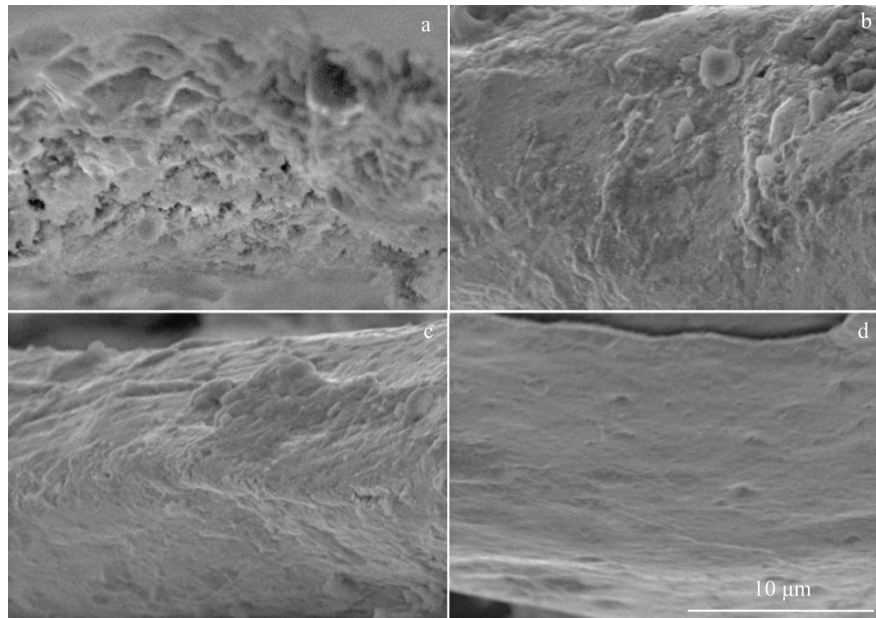


Fig.5 SEM images of torn cross-sections of copper-graphene composites with different graphene concentrations: (a) $0 \text{ g}\cdot\text{L}^{-1}$, (b) $0.3 \text{ g}\cdot\text{L}^{-1}$, (c) $0.6 \text{ g}\cdot\text{L}^{-1}$, and (d) $0.9 \text{ g}\cdot\text{L}^{-1}$

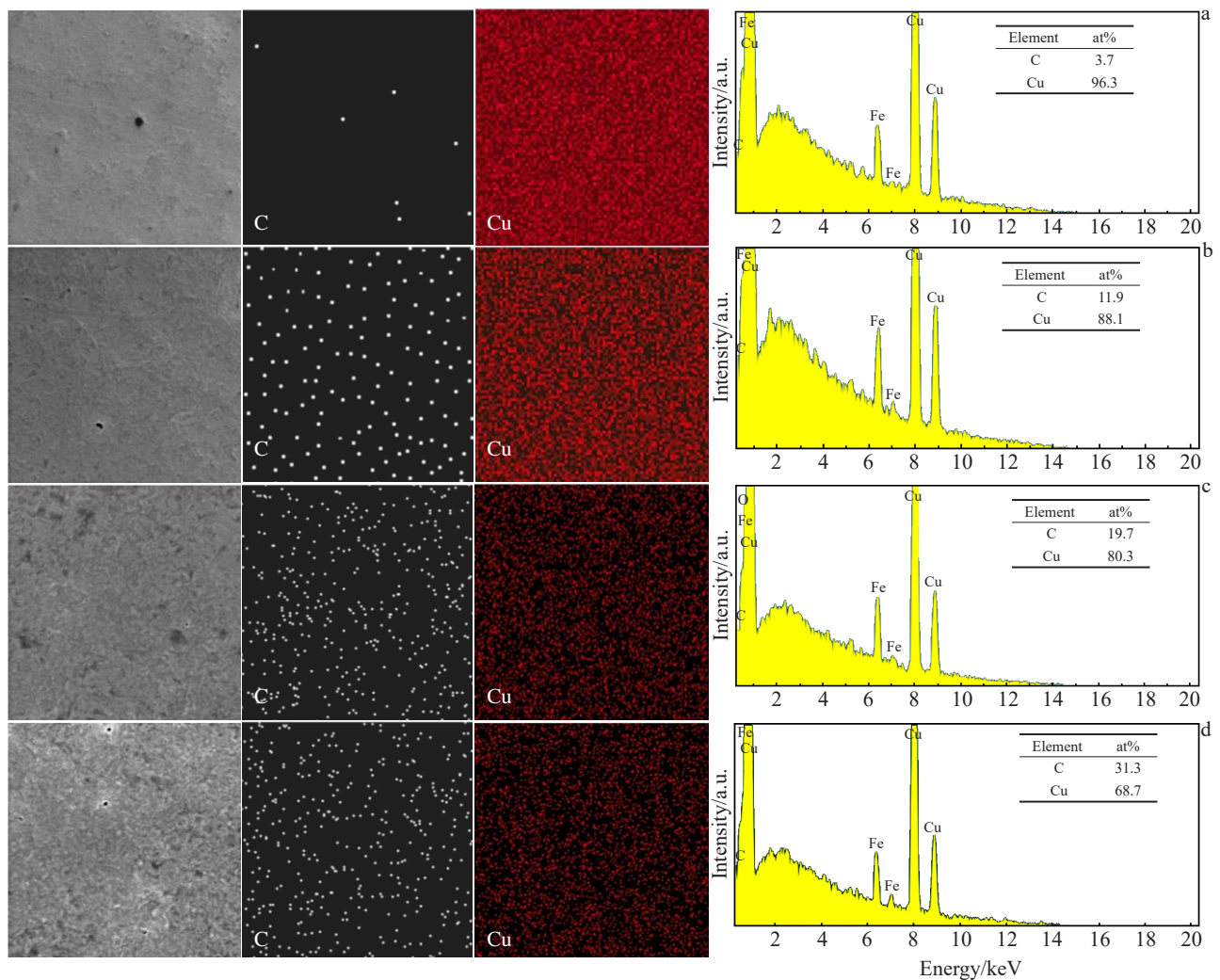


Fig.6 SEM/EDS results of element distribution and ratio of C and Cu elements in Cu-GR composites with different graphene concentrations: (a) $0 \text{ g}\cdot\text{L}^{-1}$, (b) $0.3 \text{ g}\cdot\text{L}^{-1}$, (c) $0.6 \text{ g}\cdot\text{L}^{-1}$, and (d) $0.9 \text{ g}\cdot\text{L}^{-1}$

Furthermore, the stacking of graphene in the composite was explored. Different Cu-GR composite films were etched by saturated acidic ferric chloride solution for 3 s, and the surface morphology and the ratio of C/Cu were investigated using SEM/EDS, as shown in Fig. 7. Fig. 7a shows that the electro-deposited Cu layer, which is nearly free of graphene, exhibits a loosely attached particle morphology after etching, indicating that the coating layer of pure Cu is easily eroded. For GR-containing composites shown in Fig. 7b~7d, some of the Cu particles are lost after erosion, and the corroded topography appears like a card-slotted porous morphology with increasing the graphene concentration. The composite structure is formed by the dispersion of the GR sheets into the Cu film matrix. The composite layer prepared in the plating solution with a graphene concentration of $0.9 \text{ g}\cdot\text{L}^{-1}$ was subjected to EDS test, as shown in Fig. 7d. The acquired distribution and elemental ratio of C/Cu on the eroded surface was compared with the test data of the sample before erosion (Fig. 6d). The elemental distribution of C remains unchanged after etching, while that of Cu becomes sparse, and the ratio of C:Cu increases from about 31:69 to 60:40 after erosion. This is attributed to the loss of Cu from the composite material when the surface film is etched.

At the same time, it can be found in Fig. 7 that the copper grains are refined gradually with the increase of graphene concentration. The schematic presentation of the grain refinement mechanism of copper in Cu-GR composites is illustrated in Fig. 8. In the absence of GR sheets, the electrodeposited copper particles usually grow to $0.5\sim 1 \mu\text{m}$, forming coatings layer by layer, as shown in Fig. 8a. However, when graphene sheets exist in the electrodeposition system, the uniformly dispersed GR sheets block the continuous growth of the copper grains, resulting in grain refinement effect on the obtained Cu-GR composite, as shown in Fig. 8b. And this is consistent with the phenomenon (Fig. 4) that the hardness of the composites increases with the addition of

graphene as a result of Hall-Petch strengthening^[35].

2.4 XPS characterization of Cu-GR composite coating

Different samples of Cu-GR composites were characterized by XPS, as shown in Fig. 9. The survey spectrum in Fig. 9a shows that the peak intensity of O 1s is gradually reduced with the increase of graphene concentration, indicating the gradual decrease of oxygen on the surface of the composites. Compared with raw graphene, the C 1s characteristic peak intensity of the composite is lower because the volume fraction of graphene is diluted due to the presence of Cu in the composite. As expected, most materials show obvious oxide layers and carbonaceous contamination on the surface^[36] and XPS can normally only detect depths of $5\sim 10 \text{ nm}$ ^[37,38]. Therefore, all the composite samples show significant traces of O1s and C 1s. Fig. 9b shows the C 1s fine-fitted spectrum, and the peak positions at 284.5 and 285.6 eV in the curves correspond to the Csp^2 and Csp^3 functional groups, respectively^[39]. For graphene, the Csp^2 characteristic peak intensity is the highest; and for the composite, the intensity of the Csp^2 hybridization peaks slowly increases, and Csp^3 hybridization is gradually weakened as the concentration of graphene increases. Fig. 9c shows the Cu $2\text{p}_{3/2}$ fine-fitted spectrum, and the two peak positions at 932.0 and 933.7 eV correspond to $\text{Cu}+\text{Cu}_2\text{O}$ and CuO , respectively^[40]. As the graphene concentration increases from 0 to $0.9 \text{ g}\cdot\text{L}^{-1}$, the proportion of $\text{Cu}+\text{Cu}_2\text{O}$ is found to increase, and the proportion of CuO decreases. This is consistent with the results of O 1s peaks of the composite in the XPS survey spectrum. In other words, the added graphene sheets can favor the formation of electrodeposited Cu-GR coating with low valence of Cu. The XPS results verify the composition of Cu-GR composites, and indicate that the oxygen content in the coating decreases with the addition of graphene.

2.5 Electrochemical performance of Cu-GR composite coating

It is crucial to analyze the protective performance of the Cu-

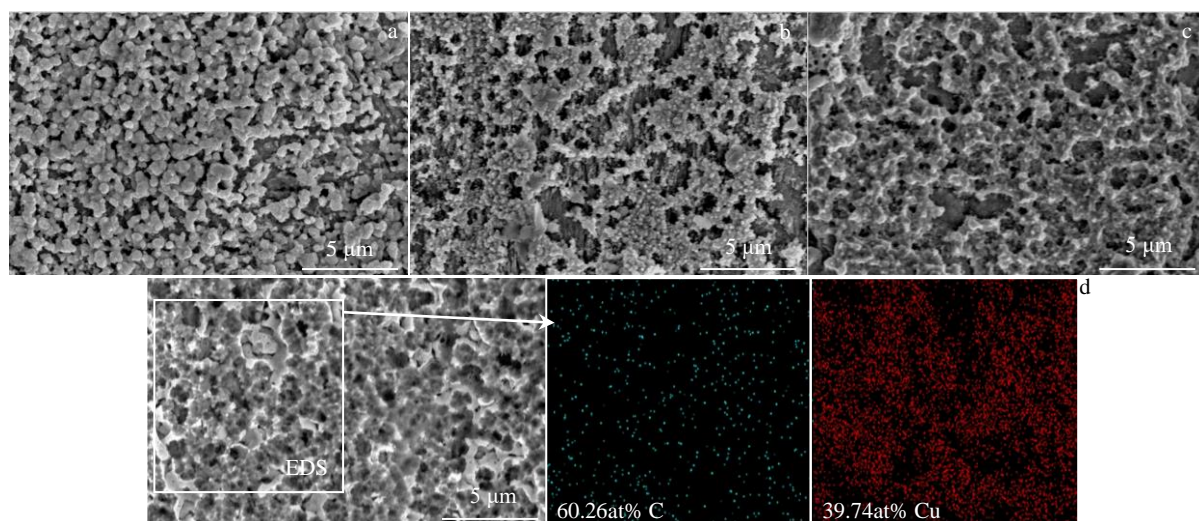


Fig. 7 SEM images of Cu-GR composites with $0 \text{ g}\cdot\text{L}^{-1}$ (a), $0.3 \text{ g}\cdot\text{L}^{-1}$ (b), $0.6 \text{ g}\cdot\text{L}^{-1}$ (c) GR sheets; SEM-EDS results (d) of Cu-GR composite with $0.9 \text{ g}\cdot\text{L}^{-1}$ GR sheet after erosion in saturated acidic ferric chloride solution

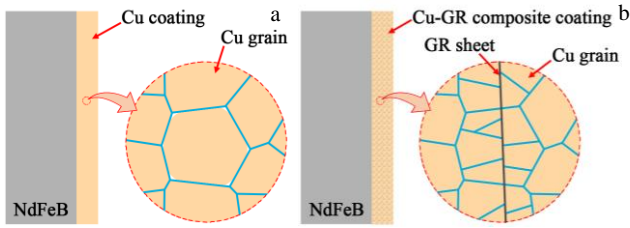


Fig. 8 Schematic presentation of the grain refinement mechanism of Cu in Cu-GR composites without (a) and with (b) graphene

GR composite coating, as an anti-corrosion coating of the sintered NdFeB surface. Corrosion resistance was analyzed via potentiodynamic polarization curves and electrochemical impedance spectroscopy (EIS). Fig. 10 shows the anode dynamic potential polarization curves of the sintered NdFeB protected by Cu-GR composite films with different graphene concentration. The polarization curves in Fig. 10a were analyzed by the polarization curve Tafel zone extrapolation method, and the corrosion potential (E_{corr}) and corrosion current density (I_{corr}) are obtained, as listed in Table 1. It can be seen that with increasing the graphene concentration, the current densities

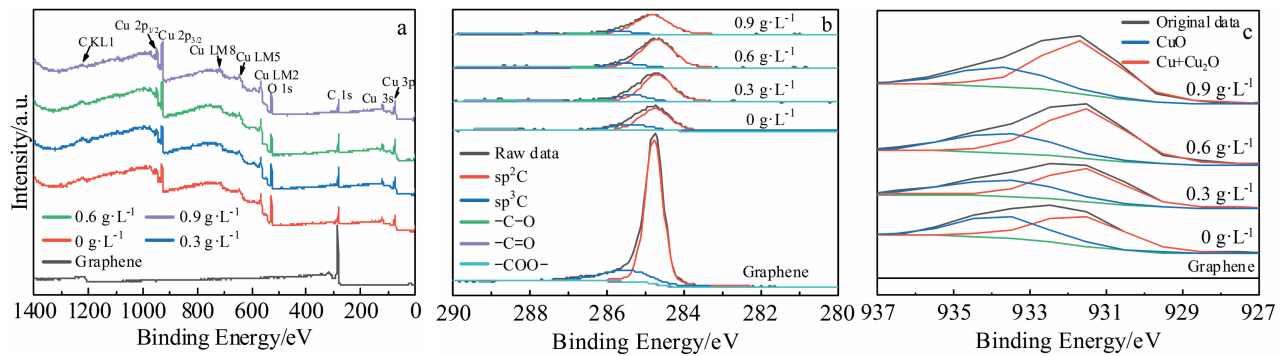


Fig. 9 XPS spectra of graphene and Cu-GR composites with different graphene concentrations: (a) survey spectra, (b) C 1s fitted spectra, and (c) Cu $2p_{3/2}$ fitted spectra

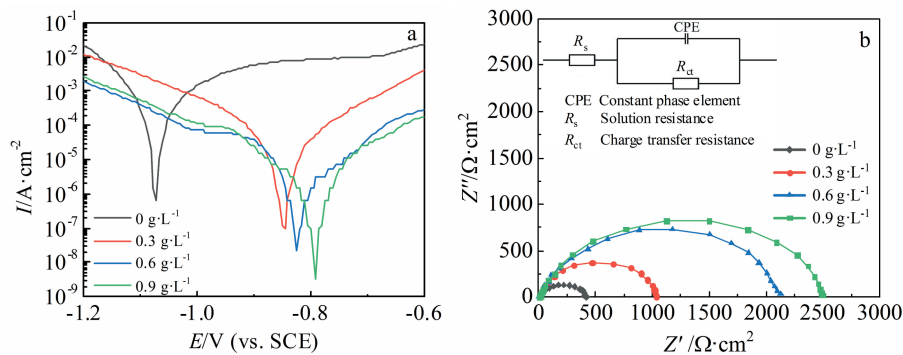


Fig. 10 Dynamic potential polarization curves (a) and EIS Nyquist plots (b) of sintered NdFeB protected by Cu-GR composite film with different graphene concentrations

and potentials corresponding to self-corrosion shift to lower and more positive values, respectively. These results indicate that the sintered NdFeB protected with the Cu-GR composite films possess more stable electrochemical performance and higher corrosion resistance than that without graphene. Fig. 10b shows the EIS Nyquist plots of sintered NdFeB protected by different Cu-GR composite films. The impedance curves show semicircular capacitance arcs and the radii increase with increasing the graphene concentration. The results are consistent with the anodic polarization test (Fig. 10a). According to the characteristics of the impedance spectrum, the equivalent circuits shown in Fig. 10b were designed to analyze the electrodeposition. Among them, CPE is the constant-phase element representing the film capacitance, R_s is the solution resistance, and R_{ct} is the film

resistance. The analysis results are listed in Table 1. The values of R_{ct} increase with the increase of graphene concentration, further supporting the fact that the Cu-GR composites possess better corrosion resistance than the Cu coating without graphene. This is consistent with the expected effects of grain refinement, improved compactness, and increased hydrophobicity.

The sintered NdFeB coated with different Cu-GR composite films were corroded by the sodium chloride solution, and the impact on the macroscopic morphology is observed, as shown in Fig. 11. The parts in the dotted circle (about $\Phi 5.5$ mm) in Fig. 11 were exposed to the corrosive solution, and the other parts of the sintered NdFeB magnets were wrapped in polytetrafluoroethylene (PTFE) container. Fig. 11a shows that in the absence of graphene, part of the

Table 1 Electrochemical analysis results of sintered NdFeB coated by Cu-GR composite with different graphene concentrations

Graphene concentration/g·L ⁻¹	Electrochemical parameters		Circuit simulation parameters		
	E_{cor}/V (vs. SCE)	$I_{\text{cor}}/\text{mA}\cdot\text{cm}^{-2}$	$\text{CPE}/\times 10^{-5} \text{F}\cdot\text{cm}^{-2}$	R_s/Ω	$R_{\text{ct}}/\Omega\cdot\text{cm}^2$
0	-1.072	6.2×10^{-4}	5.14	16.26	403
0.3	-0.845	1.0×10^{-4}	2.758	10.51	1031
0.6	-0.825	2.2×10^{-5}	3.054	12.19	2076
0.9	-0.79	3.3×10^{-6}	2.626	10.28	2407



Fig.11 Macroscopic corrosion morphologies of sintered NdFeB protected by Cu-GR composites with different graphene concentrations: (a) 0 g·L⁻¹, (b) 0.3 g·L⁻¹, (c) 0.6 g·L⁻¹, and (d) 0.9 g·L⁻¹

protective film is corroded, causing part of the NdFeB substrate to be exposed. For the NdFeB protected by the composite film prepared in the plating solution with 0.3 g·L⁻¹ graphene (Cu-GR0.3), the corrosion of the corresponding surface region is not obvious, and the composite film is almost intact, as shown in Fig. 11b. For the sintered NdFeB coated with Cu-GR0.6 and Cu-GR0.9, as shown in Fig. 11c and 11d, respectively, the composite films of the corresponding region are severely corroded and peeled off. According to the above-mentioned electrochemical performance (Fig. 10) of the Cu-GR composite coating, the corrosion resistance of the composite materials increases with the increase of graphene concentration. However, the best protective effect is obtained for Cu-GR0.3. This can be attributed to the weakened bonding force between the composite film and the NdFeB matrix as the graphene concentration exceeds 0.6 g·L⁻¹. Thus, the composite film peels off during the corrosion process, causing the internal NdFeB matrix to be exposed.

3 Conclusions

1) The Cu-GR composite coatings can be successfully fabricated on the surface of sintered NdFeB magnets using electrodeposition method, and the GR sheets are uniformly dispersed in the composite.

2) For the Cu-GR composites, as the concentration of graphene added into the plating solution increases from 0 to 0.9 g·L⁻¹, the hydrophobicity and the hardness increase due to formation of undulating structure and the refinement of Cu grain.

3) The Cu-GR composite films possess more stable electrochemical performance and improved corrosion

resistance compared with the Cu coating film without graphene.

4) The sintered NdFeB magnet coated with Cu-GR composite shows the optimal protective effect when the concentration of the GR sheets in the plating solution is 0.3 g·L⁻¹.

References

- 1 Park H K, Lee J H, Lee J et al. *Scientific Reports*[J], 2021, 11(1): 3792
- 2 Jiang W, Shen L D, Wang K et al. *Journal of Alloys and Compounds*[J], 2019, 787: 1089
- 3 Zhu W, Luo Y, Wang Z L et al. *Journal of Rare Earths*[J], 2021, 39(2): 167
- 4 Jones N. *Nature*[J], 2011, 472(7341): 22
- 5 Xu J L, Xiao Q F, Mei D D et al. *Rare Metal Materials and Engineering*[J], 2018, 47(4): 1059
- 6 Huang Y Q, Li H Q, Zuo M et al. *Journal of Magnetism and Magnetic Materials*[J], 2016, 409: 39
- 7 Nan H Y, Zhu L Q, Liu H C et al. *Rare Metal Materials and Engineering*[J], 2017, 46(12): 3658
- 8 Jakubowicz J. *Journal of Alloys and Compounds*[J], 2001, 314(1): 305
- 9 Li Q, Yang X K, Zhang L et al. *Journal of Alloys and Compounds*[J], 2009, 482(1): 339
- 10 He J Y, Liao X F, Lan X X et al. *Journal of Alloys and Compounds*[J], 2021, 870: 159 229
- 11 Xiang L, Shen Q Q, Zhang Y et al. *Surface & Coatings Technology*[J], 2019, 373: 38

- 12 Zheng J, Chen H, Cai W et al. *Materials Science and Engineering B*[J], 2017, 224: 18
- 13 Zheng J, Chen H, Cai W et al. *Journal of the Electrochemical Society*[J], 2017, 164: 798
- 14 Berry V. *Carbon*[J], 2013, 62: 1
- 15 Eda G, Chhowalla M. *Advanced Materials*[J], 2010, 22(22): 2392
- 16 Ambrosi A, Chua C K, Bonanni A et al. *Chemical Reviews*[J], 2014, 114(14): 7150
- 17 Chen J, Yao B W, Li C et al. *Carbon*[J], 2013, 64: 225
- 18 Chang K C, Hsu M H, Lu H I et al. *Carbon*[J], 2014, 66: 144
- 19 Sun W, Wang L D, Wu T T et al. *Carbon*[J], 2014, 79: 605
- 20 Singh B P, Nayak S, Nanda K K et al. *Carbon*[J], 2013, 61: 47
- 21 Chang C H, Huang T C, Peng C W et al. *Carbon*[J], 2012, 50(14): 5044
- 22 Ramezanzadeh B, Ghasemi E, Mahdavian M et al. *Carbon*[J], 2015, 93: 555
- 23 Ramezanzadeh B, Niroumandrad S, Ahmadi A et al. *Corrosion Science*[J], 2016, 103: 283
- 24 Qi K, Sun Y M, Duan H W et al. *Corrosion Science*[J], 2015, 98: 500
- 25 Yu Z X, Di H H, Ma Y et al. *Applied Surface Science*[J], 2015, 351: 986
- 26 Singh B P, Jena B K, Bhattacharjee S et al. *Surface and Coatings Technology*[J], 2013, 232: 475
- 27 Rekha M Y, Punith Kumar M K, Srivastava C. *RSC Advances*[J], 2016, 6(67): 62 083
- 28 Berlia R, Punith Kumar M K, Srivastava C. *RSC Advances*[J], 2015, 5(87): 71413
- 29 Sai Pavan A S, Ramanan S R. *Applied Nanoscience*[J], 2016, 6(8): 1175
- 30 Zhu M, Du Z, Yin Z et al. *ACS Applied Materials & Interfaces* [J], 2016, 8(1): 502
- 31 Chen S, Brown L, Levendof M et al. *ACS Nano*[J], 2011, 5(2): 1321
- 32 Liu J, Lv Y Y, Zhang Z Y et al. *Rare Metal Materials and Engineering*[J], 2017, 46(4): 888
- 33 Wu L, Wu J H, Zhang Z Y et al. *Applied Surface Science*[J], 2019, 487: 569
- 34 Guo L, Gu C, Feng J et al. *Journal of Materials Science & Technology*[J], 2020, 37: 9
- 35 Erb U, Palumbo G, Mccrea J L. *Nanostructured Metals and Alloys*[M]. Cambridge: Woodhead Publishing, 2011: 118
- 36 Meury P A, Bentouati D, Berry J J et al. *NPL Report*[R]. England: National Physical Laboratory Management Limited, 2015
- 37 Mather R R. *Surface Modification of Textiles*[M]. Cambridge: Woodhead Publishing, 2009: 296
- 38 Welker R W. *Developments in Surface Contamination and Cleaning*[M]. New York: William Andrew Publishing, 2012: 179
- 39 He W T, Zhu L Q, Chen H N et al. *Applied Surface Science*[J], 2013, 279: 416
- 40 Mai Y J, Zhou M P, Ling H J et al. *Applied Surface Science*[J], 2018, 433: 232

烧结NdFeB表面铜-石墨烯复合膜的制备与表征

陈海波^{1,2}, 郑精武¹, 付永成¹, 刘友好³, 衣晓飞³, 陈静武³, 乔梁¹,
黄秀莲³, 应耀¹, 蔡伟¹, 李旺昌¹, 余靓¹

(1. 浙江工业大学 材料科学与工程学院 磁电功能材料研究所, 浙江 杭州 310014)

(2. 浙江工业大学 机械工程学院, 浙江 杭州 310000)

(3. 安徽大地熊新材料股份有限公司, 安徽 合肥 231500)

摘要: 采用电沉积铜-石墨烯 (Cu-GR) 复合膜的方法对稀土永磁NdFeB材料进行包覆以提高其耐腐蚀性。对Cu-GR膜层的微观结构、水接触角和表面显微硬度等方面进行了分析。结果表明, 随着电沉积液中石墨烯的添加量从 $0 \text{ g} \cdot \text{L}^{-1}$ 增加到 $0.9 \text{ g} \cdot \text{L}^{-1}$, 膜层的疏水性和硬度随之提高。通过SEM/EDS和XPS表征, 验证了石墨烯在Cu-GR膜层中的均匀分散以及Cu-GR复合材料的组成。利用动电位极化曲线和电化学阻抗谱 (EIS) 研究了Cu-GR复合镀层的电化学性能。结果表明, 石墨烯的加入使膜层的电化学性能更加稳定、耐蚀性得到提高。当电沉积液中石墨烯添加浓度为 $0.3 \text{ g} \cdot \text{L}^{-1}$ 时, 获得的Cu-GR复合包覆层在NdFeB基体上表现出最优的综合保护效果。

关键词: 铜-石墨烯; 复合物包覆; 耐腐蚀性; NdFeB

作者简介: 陈海波, 男, 1990年生, 博士, 浙江工业大学材料科学与工程学院, 浙江 杭州 310014, 电话: 0571-88320450, E-mail: chenhibo@foxmail.com